

A Consequent-Pole Hybrid Exciter for Synchronous Generators

Stefano Nuzzo, *Member, IEEE*, Paolo Bolognesi, *Member, IEEE*, Giovanni Decuzzi,
Paolo Giangrande, *Senior Member, IEEE*, Michael Galea, *Senior Member, IEEE*

Abstract— In low-to-medium power generating sets, a self-powered brushless excitation system is typically employed. This solution is cost-effective, simple and compact, but it suffers from an unreliable voltage build-up at start-up, a slow dynamic response and a relatively low efficiency for the exciter. The push towards more effective, reliable and efficient products has recently led to consider excitation systems equipped with permanent magnet exciters and controlled rotating converters, but their diffusion is limited by their higher complexity and cost. This paper investigates the utilization of a hybrid excitation for the exciter, aiming to join the benefits of field windings and permanent magnets. As a case study, this concept is applied to a mid-size industrial generating set. After a preliminary analysis, a consequent-pole layout with surface-mounted bonded magnets is selected as the most effective solution in an industrial perspective, since it permits to maximize the benefits while minimizing the required modifications in the system design. Theoretical considerations, numerical analysis and experimental validation are reported to show that the hybrid excitation concept can actually lead to a significant reduction of the exciter field losses as well as to other appreciable side benefits with a very limited impact on the present design of the generating set.

I. INTRODUCTION

THE general trend in the design of electrical machines is presently towards more efficient, power-dense and reliable solutions. This has determined a growing interest also in renewing and revamping the design of classical machines such as wound-field synchronous generators (WFSGs) [1]-**Error! Reference source not found.**

Apart from their traditional role, i.e. grid-connected electrical generation in large power plants [5], WFSGs are also very important in small-to-medium power generating sets (gensets) intended to supply isolated loads and/or for standby/emergency applications [2]. In these applications, self-sufficiency, robustness, commissioning simplicity, minimal maintenance requirements and low cost are key features. These characteristics are matched nowadays pretty well by the popular brushless excitation system (ES), which is then by far the most preferred choice. Its typical configuration comprises a 3-phase inverted-layout auxiliary WFSG used as exciter, whose stationary field winding is supplied and controlled by an

automatic voltage regulator (AVR). The rotating armature of the exciter supplies a full-bridge diode rectifier located on the rotor and feeding the field winding of the main alternator (MA), which is a WFSG featuring a conventional layout and typically a 3-phase armature. While this architecture is widely used, it was recently shown that some aspects (e.g. the voltage drop ensuing from the diode commutations [6]) are still overlooked, thus often resulting in over-engineered exciters **Error! Reference source not found.** Other drawbacks of the conventional brushless ES include: a) the AVR is supplied by the armature of the MA (i.e. the system is self-excited) and is therefore inherently affected by its operative conditions, especially during large transients [8]; b) during the start-up process of the genset, the voltage build-up only relies upon the residual magnetism in the rotor core, thus resulting relatively slow and not fully reliable.

To overcome such drawbacks, especially in mid-large gensets a pilot exciter, whose excitation is provided by permanent magnets (PMs), is often added to supply the AVR as soon as the genset rotates at its minimum design speed. However, this solution leads to a larger, heavier and more expensive system. The combined design of a PM pilot + main exciter pair has been proposed in [9] to achieve both the compactness typical of self-excited ES and the voltage build-up benefits associated with separately-excited systems.

Recently, the use of PMs directly for the main exciter has been also proposed to eliminate the pilot exciter. However, such solution entails the replacement of the passive diode rectifier with some sort of actively controlled converter **Error! Reference source not found.** to permit adjusting the field winding current of the MA. Besides allowing to eliminate the Joule losses in the exciter field winding, combining PM exciters and rotating controlled converters may provide some additional benefits compared to the classical scheme. These include a faster dynamic response, a reduced ripple in the current fed to the MA field winding and an improved controllability. Nevertheless, most manufactures are still reluctant to adopt significant variations in the traditional designs of small-to-medium-size genset, due to their higher complexity and production cost.

This paper investigates a different solution consisting in using an exciter featuring a hybrid excitation, i.e. equipped with

S. Nuzzo is with the Department of Engineering Enzo Ferrari, University of Modena and Reggio Emilia, Modena, Italy (e-mail: stefano.nuzzo@unimore.it) and with the Power Electronics, Machines and Control Group, University of Nottingham, Nottingham, UK (e-mail: stefano.nuzzo@nottingham.ac.uk).

P. Bolognesi is with the Electric Machines, Power Electronics and Drives group of the Department DESTEC, University of Pisa, Pisa, Italy (e-mail: p.bolognesi@ieee.org).

G. Decuzzi was with the University of Pisa, Italy, on leave at the University of Nottingham, UK (e-mail: giovanni.decuzzi2@positech.it).

P. Giangrande and Michael Galea are with the Power Electronics, Machines and Control Group, University of Nottingham, Nottingham, UK (e-mail: p.giangrande@nottingham.ac.uk and michael.galea@nottingham.ac.uk).

M. Galea is also with the Power Electronics, Machines and Control Group, University of Nottingham Ningbo, Ningbo, China (e-mail: michael.galea@nottingham.edu.cn).

both PMs and field winding. The proposed concept is applied for upgrading the existing exciter of an industrial genset, which is presented as a case study. A hybrid-excited machine joins the benefits of both the two main types of ESs above recalled. In fact, on one hand it maintains the high compactness, the low system complexity and the limited production cost typical of ESs including wound-field exciters and diode rectifiers, like the one considered as case study. On the other hand, thanks to the embedded PMs, it achieves a significant reduction of the exciter field losses and features a fully reliable voltage build-up just as the ESs equipped with an additional pilot exciter, without requiring neither the latter nor a rotating controllable converter.

The hybrid excitation concept has been already successfully proposed in the past for different types of machines [11]-[13], including dual stator **Error! Reference source not found.** and flux switching [14] machines. Neither the hybrid excitation, nor the consequent-pole arrangement **Error! Reference source not found.**, nor the combination of these two features **Error! Reference source not found.** are new concepts by themselves. Nevertheless, no proposals or relevant results are reported in the available literature about the utilization of hybrid excitation solutions in exciters for small-to-medium size gensets. This paper investigates such application introducing the concept and discussing the selection of the operating point for the PMs (Section II) referring to the modification of an existing industrial genset as a case study (Section III). The methodology leading to the final design of a consequent-pole structure is presented with the expected performance (Section IV) and the realization and testing of a prototype are then described (Section V). Final considerations are then presented (Section VI) highlighting the potential benefits of the proposed solution compared to conventional configurations.

II. PROPOSED CONCEPT

In Fig. 1, the block scheme of the genset considered as case study is illustrated. It comprises a $400kVA$, $400V$, $50Hz$, 3-phase salient-pole MA and a conventional brushless ES composed of a wound-field exciter, a rotating diode rectifier and an AVR.

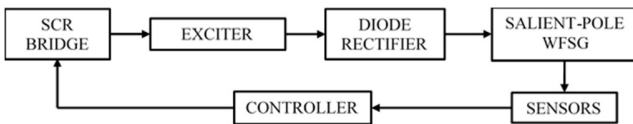


Fig. 1. Architecture of the industrial genset considered as case study.

The focus of this paper is on the exciter, which is a 3-phase inverted-layout rotating-armature WFSG designed to provide $\approx 5kW$ to the field winding of the MA when it operates at rated load. The exciter field winding is wound around the stator poles, whereas the armature coils are deployed in a single-layer layout resulting in a simple full-pitch, 1 slot-per-pole-per-phase winding arrangement. To feed and regulate the average current in the exciter field winding, the AVR is equipped with a single-phase, half-wave controlled rectifier consisting of 1 SCR and 1 diode connected in anti-parallel to the load to provide a freewheeling path for the MA field current when the SCR is not conducting. The main characteristics of the MA and of the exciter are summarized in Table I.

The key idea investigated in this paper consists in using the PMs to provide an appropriate “basic level” in the excitation flux of the exciter and thus in the current provided to the MA field winding, while the capability to regulate the value of such

current is still fully retained by properly adjusting the field current of the exciter, similarly to classical brushless ESs. Depending on the application, the most convenient operating condition of the MA can be selected for defining such basic level and thus for sizing the PMs accordingly.

TABLE I
Main parameters of Alternator and Exciter

	Alternator	Exciter
Rated Power [kVA]	400	5.35
Line-to-line rated Voltage [V_{rms}]	400	75
Rated Frequency [Hz]	50	175
Pole Number	4	14
Armature Slot Number	48	42
Magnetic Laminations	M700-65A	M700-65A
Field winding resistance @ $20^{\circ}C$ [Ω]	1.35	18

A. Design Guidelines

The industrial partner providing the benchmark genset highlighted that nowadays such products are rather mature and are sold in a rather price-sensitive market, meaning that the actual chances of adoption of the proposed solution were strictly related to the minimization of any adverse impact on the existing design. Therefore, as in-detail discussed in Section IV.A the minimization of the manufacturing complexity and cost was assumed as the main guideline for the design.

In particular, the industrial genset considered in this paper is designed to operate supplying widely variable ohmic-inductive passive loads at rated voltage and frequency (and thus speed). In such conditions, the armature reaction in the MA always produces a voltage drop, meaning that the field current required to keep the output voltage at its rated level is always greater or equal than the value producing such voltage at no load. In turn, this implies that the excitation flux in the exciter never falls below the value required to reach the rated voltage of the MA at no-load. Hence, according to the design guideline above illustrated, the most convenient choice consists in sizing the PMs in such a way that, when the field current in the exciter is zero and no load is connected to the MA, its output voltage assumes the rated value. This allows to keep unmodified the converters presently used in the benchmark genset, i.e. both the rotating diode bridge and the unidirectional SCR-based rectifier in the AVR, thus limiting the modifications with respect to the benchmark genset.

III. ANALYSIS OF THE BENCHMARK EXCITER

Aiming to pave the way for the accurate design of the PM-field winding machine, it is deemed essential to develop and validate a finite-element (FE) model for the benchmark exciter. In this section, such model is then detailed and relevant results are compared to corresponding experimental data for validation. Once the validity of the FE model is confirmed, it is slightly updated before being used for the hybrid exciter design.

A. Simulation Model

In the considered case study, the axial length of the exciter is $50mm$ whereas the external diameter is $500mm$, giving a rather low 1:10 ratio, which suggests to keep into account the end effects. Rather than developing a 3D model which would be

computationally expensive, the analysis can be carried out using a 2D FE model coupled with an auxiliary circuitual part, where the active sides of the modeled coils (labeled $Coil_S$ and $Coil_R$ for stator and rotor windings respectively in the scheme depicted in Fig. 2) are properly connected each other and to any other circuitual element eventually required. In particular, the 3D end effects are taken into account by including in the circuit some appropriate resistors (R_{S_3D} and R_{R_3D} for stator and rotor respectively) and inductors (L_{S_3D} and L_{R_3D} for stator and rotor respectively), as shown in Fig. 2. The values of such elements were estimated according to [17] and can be found in **Error! Reference source not found.** for the exciter under analysis.

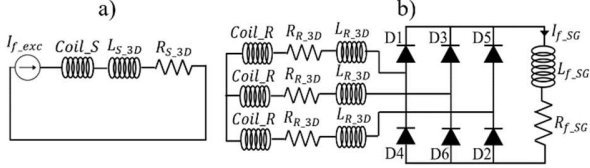


Fig. 2. Circuit coupled to the 2D FE model of the exciter: a) stator b) rotor

According to the specific operating condition to be simulated, and considering the way the related experimental tests were actually performed, either a current or a voltage DC source was used to feed the exciter field winding. In Fig. 2 a constant current generator is shown.

The load fed by the exciter through the rotating rectifier consists of the field winding of the MA. Although in general more complex phenomena take place, under normal steady-state conditions the MA field winding can be approximately modeled through the equivalent resistance R_{f_SG} and self-inductance L_{f_SG} , as observed in Fig. 2. However, if the real value of the self-inductance of the MA field winding was used in the model (i.e. $\approx 4H$ for the considered case study), a large time constant L_{f_SG}/R_{f_SG} would be obtained (about 3s), thus requiring a very long time to achieve steady-state. Therefore, after a sensitivity analysis aimed at finding an optimal trade-off between accuracy and computational burden, a simplified representation was adopted consisting in modeling the MA field winding as an ideal constant current generator, whose value is chosen coherently with the operating conditions targeted.

Concerning the FE model itself, the inherent odd angular symmetry of the 14-poles structure of the machine was exploited by modeling only an angular sector corresponding to 1 pole pitch. A 2D cross section of the FE model developed for the benchmark exciter is shown in Fig. 3, featuring the single coil side per each armature phase in the rotor as well as the field coil obtained by merging for the sake of simplicity the 2 actual coil sides wound around the 2 adjacent stator poles.

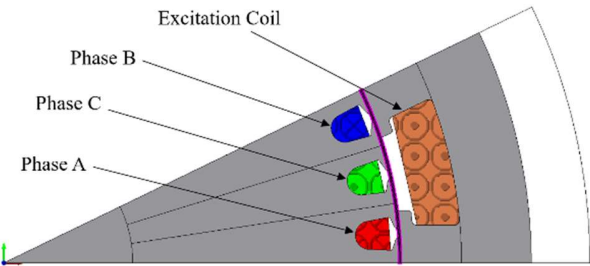


Fig. 3. 2-D FE model of the benchmark exciter (1/14 of the whole machine).

B. Simulation results and experimental validation

The precursor of the FE model adopted in this paper was already validated in **Error! Reference source not found.** referring to the benchmark machine. In that study, the good agreement between simulation results and experimental measurements was proved by examining 1) the no-load characteristic, 2) the self and mutual-inductances of the armature phases and 3) the voltage drop ensuing from the diodes' commutations in the rotating rectifier. Hereafter, additional comparisons between simulation results and experimental data are presented to further prove the validity of the model also for the sake of this investigation.

First, the no-load voltages generated at rated speed (1500rpm) at the exciter armature terminals (i.e. with the MA field winding disconnected from the rectifier DC output) for a significant value of field current (i.e. 1A) are compared in Fig. 4 in terms of waveforms and related low-frequency amplitude spectrum. A very good match between simulation and experimental results can be observed.

A second comparison is performed when the genset rotates at rated speed and the exciter field current is set to an appropriate value (0.64A) such that the rotating rectifier feeds the MA field winding with the DC current (14.6A) producing the rated line-to-line voltage (400Vrms) at no load. This operating point represents just the “basic level” selected for sizing the PMs in the hybrid exciter (see Section II.A) and is therefore considered the most relevant exciter on-load condition to be analysed for the purpose of this paper. The voltage waveforms obtained from simulations and measurements in such conditions at the DC output of the rotating rectifier are compared in Fig. 5. A very good agreement is observed in terms of both average values (21.8V FE vs. 21.2V experimental) and waveform shape, thus confirming the validity of the FE model.

The availability of an experimentally proven FE model for the benchmark exciter provides a solid ground for developing a similar FE model for the derived hybrid exciter, which can be then used to validate and refine the proposed design.

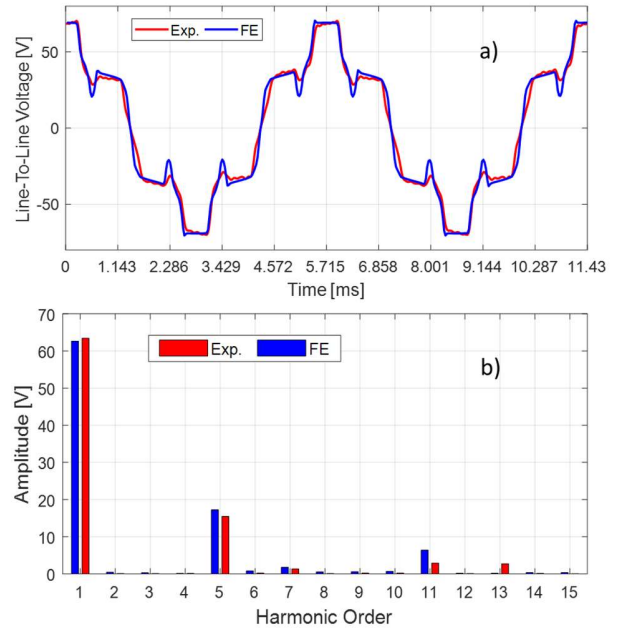


Fig. 4. Comparison between FE and experimental line-to-line armature voltages generated by the benchmark exciter at rated speed (1500rpm) with null phase currents and field current equal to 1A: a) waveforms, b) spectra.

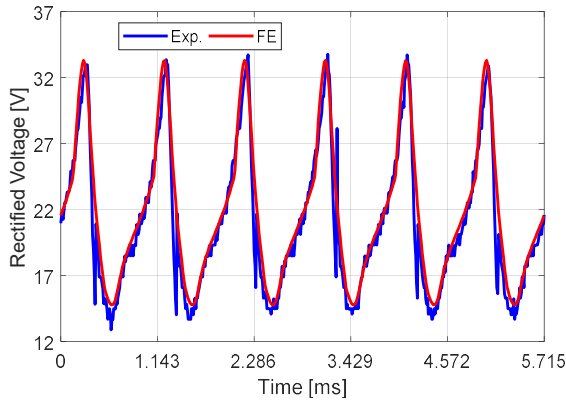


Fig. 5. Comparison between FE and experimental waveforms of the output voltage provided by the rotating rectifier at rated speed when the exciter and alternator field currents equal to 0.64A and 14.6A respectively, generating the MA rated voltage at no load.

IV. DESIGN OF THE HYBRID EXCITER

In this section, the design procedure of the hybrid PM – field winding exciter is presented. First, considerations and targets for the preliminary design are presented. Then, the validated FE model above recalled is updated to include the PMs and is used to analyze a number of possible design solutions aiming to identify the optimal one. The steps leading to the final selection of a consequent-pole hybrid-excited topology are then detailed. The iterative process adopted is summarized in the flowchart shown in Fig. 6.

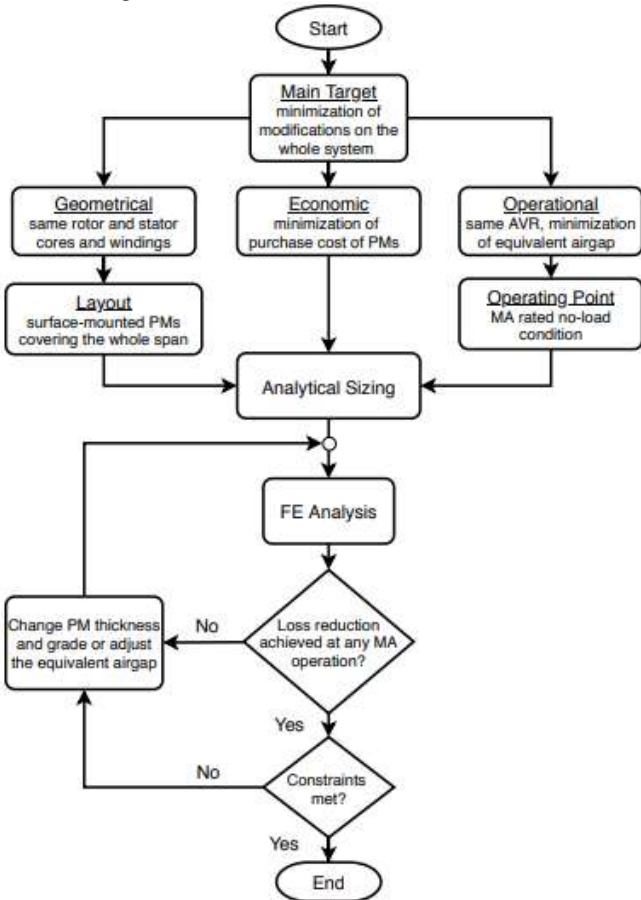


Fig. 6. Flowchart of the iterative design process

A. Preliminary design considerations and constraints

As mentioned in Section II.A the minimization of any disruptive modification to the present benchmark ES was assumed as the main target for the design of the proposed hybrid exciter, aiming to increase the chances of its practical implementation according to the recommendations from the industrial partner. The following guidelines, based on geometrical, economical and operational considerations, were then assumed for the design of the hybrid exciter:

- 1) the rotor was kept identical to the benchmark exciter;
- 2) the thickness of the mechanical airgap was maintained the same as in the benchmark exciter (1mm);
- 3) the stator was kept identical to the benchmark exciter, apart from the features required to host the PMs: a simple surface-mounted layout was then chosen, assuming to glue the PMs onto the gap-facing surface of the pole shoes;
- 4) the PM material was wisely selected to minimize the impact on the production costs;
- 5) the no-load, rated voltage condition of the MA was chosen as the “basic supply” provided by the PMs, according to the considerations in Section II.A.
- 6) the overall design had to be able to reduce the excitation power required at any other operating condition of the MA, up to full load.

Therefore, the only planned modifications in the genset design with respect to the existing structure consist in increasing the bore diameter of the stator laminations and in gluing the PMs on the main surfaces of the stator poles of the exciter. However, increasing the internal diameter of the stator core determines a thicker equivalent magnetic gap. This means that, when such challenge is not properly addressed, in case an excitation boost is required during the on-load operation of the MA, the corresponding values of field current in the hybrid exciter could turn out even greater than those in the benchmark machine, in contrast to objective 6). Therefore, the thickness of the PMs has to be minimized while matching the target of achieving the selected “basic supply” condition.

Concerning the selection of the PMs, according to objective 4), a cheap material featuring poor magnetic properties may appear as the best solution at first. However, for any desired flux level, the poorer the magnetic properties, the thicker the PMs, thus leading to a larger equivalent magnetic gap which could raise the same issue highlighted above. On the other hand, exciters for mid-low power gensets (as the benchmark machine) are often designed to operate with rather low flux density levels in the airgap **Error! Reference source not found.** When the same scenario has to be replicated using powerful rare-earth PMs, their design thickness may then result very thin and thus challenging to manufacture. An appropriate selection of the PM material plays then a significant role in the design of the proposed hybrid solution.

B. Analytical sizing

Having identified the design guidelines, including the location and layout of the PMs, the sizing procedure can begin aiming to produce the same value of airgap flux density as in the benchmark machine at the selected “basic supply” condition, i.e. the rated no-load operation of the MA.

According to [18], in the airgap of any rotating machine equipped with surface-mounted PMs, the average radial flux density B_G can be related to the magnetic field strength H_G via

the constitutive equation (1), where \bar{i} is the vector of currents entering the machine phases, α is the angular position of rotor vs. stator, λ is a normalized coordinate mapping the whole airgap along the tangential direction, μ_0 is the permeability of vacuum. According to (2), H_G can be determined as the ratio of the equivalent magneto-motive force (m.m.f.) F_E to the equivalent airgap thickness ε_E given in (3).

$$B_G(\lambda, \alpha, \bar{i}) = \mu_0 H_G(\lambda, \alpha, \bar{i}) \quad (1)$$

$$H_G(\lambda, \alpha) = \frac{F_E(\lambda, \alpha, \bar{i})}{\varepsilon_E(\lambda, \alpha)} \quad (2)$$

$$\varepsilon_E(\lambda, \alpha) = \varepsilon_G(\lambda, \alpha) + \varepsilon_M(\lambda, \alpha) \frac{r_G(\lambda, \alpha) \mu_0}{r_M(\lambda, \alpha) \mu_M} \quad (3)$$

In (3), μ_M is the relative permeability of the PMs; $\varepsilon_G(\lambda, \alpha)$ and $\varepsilon_M(\lambda, \alpha)$ are functions providing the magnetic thickness of the mechanical airgap and of the PMs, respectively; $r_G(\lambda, \alpha)$ and $r_M(\lambda, \alpha)$ are the radii of the mean magnetic surfaces inside the mechanical airgap and the PMs, respectively. Therefore, in the benchmark exciter $\varepsilon_E(\lambda, \alpha) = \varepsilon_G(\lambda, \alpha)$ since no PMs are present.

When the same “basic supply” operating condition is desired for both the hybrid and the benchmark machines, the same airgap flux density levels should be achieved. In the benchmark exciter, the equivalent value of stator m.m.f. is given by multiplying its excitation current value I_{exc} by the equivalent field winding function $N_{exc}(\lambda, \alpha)$. In the hybrid exciter, the field current is null for the considered basic condition, meaning that only the PMs provide a contribution to the equivalent m.m.f. This is given by the product of their virtual coercive force H_{CB} by their thickness $\varepsilon_M(\lambda, \alpha)$. Therefore, by imposing the equality between the $B_G(\lambda, \alpha, \bar{i})$ expressions determined for both exciters, equation (4) can be obtained.

$$\frac{N_{exc}(\lambda, \alpha) I_{exc}}{\varepsilon_G(\lambda, \alpha)} = \frac{H_{CB} \varepsilon_M(\lambda, \alpha)}{\varepsilon_G(\lambda, \alpha) + \varepsilon_M(\lambda, \alpha) \frac{r_G(\lambda, \alpha) \mu_0}{r_M(\lambda, \alpha) \mu_M}} \quad (4)$$

In (4), the left side is well known as it refers to the benchmark exciter. The parameters to be selected for the design of the hybrid exciter are therefore $H_{CB}(\lambda, \alpha)$, $\varepsilon_M(\lambda, \alpha)$ and $r_M(\lambda, \alpha)$, which are related to the PMs. In particular, the first two quantities are mostly significant, since the third one will be dominated by the fixed bore diameter assumed for the stator structure.

C. Initial design of the hybrid exciter

According to the guidelines, in the first design exercise it was assumed that all stator poles are equipped with a layer of PMs featuring the same thickness and same coercive field with radial magnetization. Considering the benefits of minimizing the equivalent airgap increase, a thickness of $0.5mm$ was initially considered for the PMs, leading to a uniform equivalent airgap thickness of about $1.5mm$. Under such assumptions, (4) permits to estimate the required value of H_{CB} in the range of $500-600kA/m$. These values are compatible with low-end and bonded variants of Samarium-Cobalt (SmCo) and Neodymium-Iron-Boron (NdFeB) rare-earth materials. As reported in **Error! Reference source not found.**, such a preliminary solution was investigated by properly adapting the FE model validated for the benchmark exciter to include the PMs, keeping all of the major features described in Section III.A. Although the above analysis showed very promising results in the whole range of operating conditions of the MA, a preliminary

assessment of the practical feasibility of the designed solution, involving inquiring manufacturers of PMs, highlighted some challenges. In fact, the very thin non-standard thickness assumed for the PMs ($0.5mm$) turned out to be challenging to manufacture. Therefore, the PM thickness was increased up to the minimum value suggested by the manufactures, i.e. $1mm$. Accordingly, the resulting value of H_{CB} was reduced to $\approx 300-400kA/m$, i.e. compatible also with high-end hard ferrites, but in the end such materials were ruled out as still difficult to manufacture in such a thin thickness. On the other hand, from a thermal point of view, temperatures in the order of $60^\circ C$ were experimentally recorded in the benchmark exciter field winding during rated full-load operation of the MA, thus excluding any need for PMs able to operate at high temperature. Therefore, SmCo was also ruled out.

Bonded NdFeB magnets (BNP-6 type) with a radial thickness of $1mm$ were then finally selected, featuring the properties listed in Table II. It is worth noting that the high electric resistivity featured by such material permits to neglect the eddy currents inside the PMs for the sake of this investigation.

TABLE II
Main Properties of Selected Bonded NdFeB Material

Remanence B_r [T]	0.55-0.62	Temp. Coeff. of H_{cj} $\alpha(H_{cj})$ [%/°K]	-0.35
Coercivity H_{cb} [kA/m]	285-370	Recoil Permeability μ_{rec}	1.15
Intrinsic Coercivity H_{ci} [kA/m]	600-755	Curie Temperature T_c [°C]	300
Average Resistivity [mΩcm]	5.6	Max. Operating Temp. T_w [°C]	130

The designed solution was checked first via FE analysis, aiming to confirm that the selected “basic supply” condition was correctly achieved. Therefore, the MA rated no-load condition was then examined while the exciter field current was set to zero (i.e. the PMs contribution only was considered). The results revealed that the rectifier output voltage waveform is very similar to that of the benchmark genset, plotted in red in Fig. 5, yet with average value $\approx 4\%$ lower. While this first check was passed, the drawbacks discussed in Section IV.A due to the increased equivalent magnetic airgap were highlighted. In fact, in such a configuration, the equivalent airgap thickness becomes $\approx 2mm$ ($1mm$ mechanical airgap + $1mm$ PMs) and the FE analysis showed a $\approx 6\%$ increase in the exciter field current required to support the MA full-load rated operation.

D. Final consequent-pole configuration of the hybrid exciter

Relying on the above results, a promising solution aimed to reduce the negative effect of the equivalent gap increase in the hybrid exciter was singled out, consisting in adopting a consequent-pole surface-mounted PM layout **Error! Reference source not found.** In such topology, only one stator pole in each pair (e.g. only the 7 North-oriented poles) is equipped with PMs, whereas the other 7 poles are left unaltered as in the benchmark machine. Thanks to this arrangement, the minimum thickness limit of $1mm$ for the PMs involves a potentially smaller increment of the equivalent airgap. Aiming to fully exploit such opportunity while still using the inexpensive bonded PMs previously selected, the reference

level assumed for the “basic supply” target was also somewhat reduced. This implies that some field current will be required even to obtain the rated voltage output from the MA at rated speed and no-load. However, in the end this choice was reputed to be the most convenient since it permits to achieve in any condition a reduction of the field current, with a more significant gain at higher load values which are more likely to be faced by the genset during its operation. A summary of the main characteristics of the consequent-pole hybrid exciter derived by the above design process is reported in Table III.

TABLE III
Main parameters of the Consequent-Pole Hybrid Exciter

Nameplate data and materials		Geometrical characteristics	
Rated Power [kVA]	5.35	Outer diameter [mm]	500
Full-load armature voltage [V _{rms}]	75	Axial length [mm]	50
Rated Frequency [Hz]	175	Rotor diameter [mm]	168.5
Pole Number	14	PM thickness [mm]	1
Armature Slot Number	48	Pole Number	14
Magnetic Laminations	M700-65A	Armature Slot Number	48
PM material	BNP-6	Slots-per-pole-per phase	1

E. Simulation model and results for the proposed exciter

Since the consequent-pole layout of the hybrid exciter is not significantly different from the structures previously analyzed, the considerations presented in Section III.A are still applicable, meaning that a 2D FE model with associated circuit part is suitable to analyze also the proposed machine. On the other hand, the latter does not feature an odd-periodic symmetrical layout as the benchmark exciter. Therefore, in this case the even-periodic symmetry related to the 7 existing pole pairs dictates the minimum extension of the modeled region, i.e. 2 pole pitches. The geometry of the 2D FE model of the proposed consequent-pole structure is reported in Fig. 7, where an in-zoom of a stator tooth hosting a PM (in yellow) is also highlighted. All of the major features of the circuit part are kept the same as in Fig. 2.

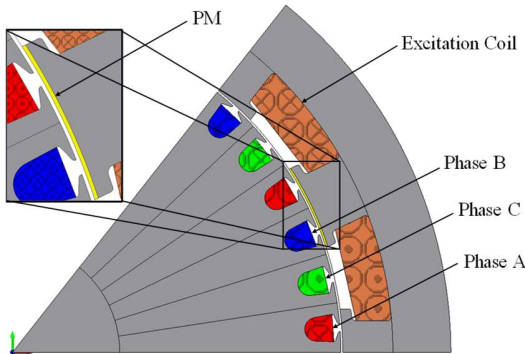


Fig. 7. 2-D cross section of the consequent-pole hybrid exciter FE model (1-7th of the whole machine).

In Fig. 8, the field maps related to 4 different operating conditions of the hybrid exciter at rated speed are reported in the same shaded colors scale: a) no current fed to the rectifier; b) no-load, rated output voltage for the MA; c) 50% of loading of the MA at rated voltage; d) full rated condition of the MA. A very small difference is observed between a) and b) conditions,

meaning that the armature reaction effect in the exciter is negligible at the selected “basic supply” operating point. A more significant effect is seen in Figures 8.c and 8.d, but even at full-load the impact of the armature reaction on the magnetic conditions is limited. Further results provided by the FE model are presented in Section V in comparison with experimental data obtained from a purposely-built full-scale prototype.

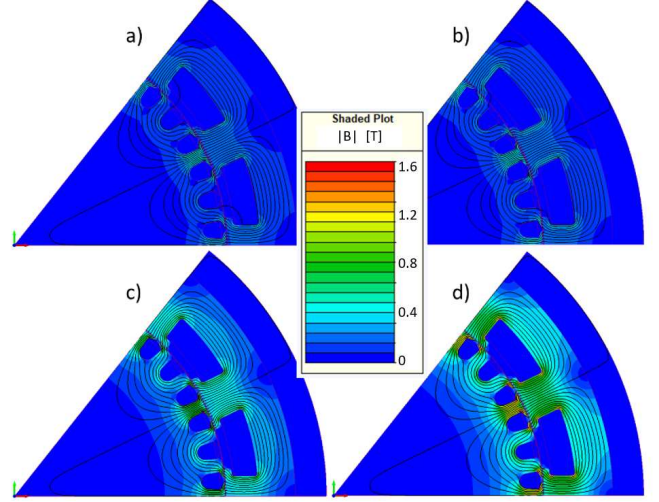


Fig. 8. Field map and flux lines distributions of the hybrid exciter at a) no-load operation of the exciter, b) rated no-load condition of the MA, c) 50% of loading of the MA at rated voltage and d) rated full-load operation of the MA.

F. Temperature influence and demagnetization analysis

While the simulations above recalled were carried out assuming cold conditions (environment temperature, i.e. 20°C) for the genset, the proper operation of the proposed hybrid excitation was also verified considering the degradation of the PM properties at the rated operating temperature measured in the exciter stator (i.e. 60°C). The performance curves for the selected PM material are shown in Fig. 9 for different temperatures. The equivalent linearized PM properties at 60°C were estimated by using the temperature coefficient listed in Table II. According to its relatively low value and to the modest temperature rise $\Delta T=40^\circ\text{C}$, no significant difference was spotted in the results compared to the cold condition scenario.

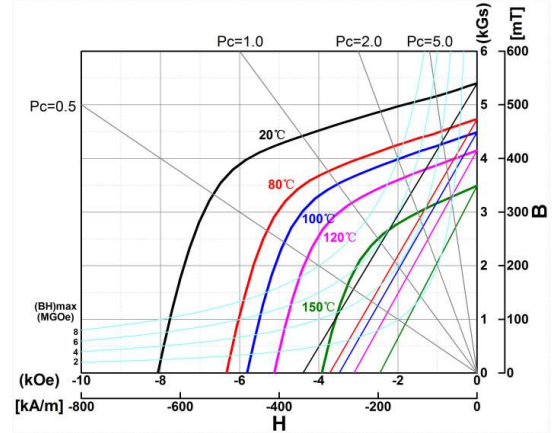


Fig. 9. Demagnetization curves at various temperatures of the selected bonded NdFeB PMs (BNP-6 type).

In addition, the risk of demagnetization of the PMs due to excessive reverse field was assessed under critical operating

conditions. The real PM demagnetization curves are linear for the whole range of temperatures reported in Fig. 9, meaning that the demagnetization knee is located in the third quadrant. This is also obviously true for the curve related to 60°C, although the latter is not shown in the figure.

Referring to the curves in Fig. 9, the value of the P_c ratio between magnet and airgap thicknesses is approximately equal to 1 in the considered design. When current flows in the exciter field winding, with a direction always aimed to increase the flux density to compensate for the voltage drop due to the armature reaction, the operating point of the PMs is expected to be pushed even further back from the demagnetization knee. To further validate the above conclusions, FE simulations were carried out both at full-load and short-circuit conditions, using the PM properties related to 60°C. This corresponds to the worst-case scenario, considering that the expected loss reduction would correspondingly lead to lower operating temperature in the exciter stator, as actually confirmed by the experimental tests (see Section VI) which showed a steady-state temperature of $\approx 50^\circ\text{C}$. The “demagnetization prediction” tool provided by the FE software was then used to spot any related potential risk. As seen in Fig. 10, such a risk was not highlighted at any simulated time instant in both of the examined conditions. These results, together with the margin between the recorded operating temperature and the maximum operating temperature for the PMs declared by the manufacturer (i.e. 130°C – see Table II), lead to safely conclude that no demagnetization may occur neither during normal operation nor under anomalous conditions.

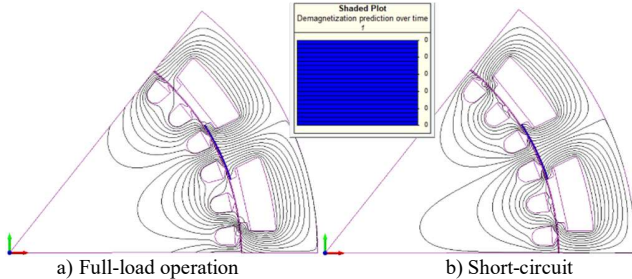


Fig. 10. Demagnetization prediction over time for the PMs at a) full-load operation of the MA and b) short-circuit at the exciter armature terminals.

IV. PROTOTYPING AND EXPERIMENTAL VALIDATION

A. Prototype

Aiming to minimize any discrepancy with respect to the considered benchmark genset, a consequent-pole hybrid machine was manufactured by simply modifying an available specimen. The gap-facing surface of 1 stator pole in each pair was then properly milled to host the PMs.

The magnet volume planned to be used in each modified stator pole was segmented, as customary. However, given the negligible eddy currents losses predicted in the PMs, the segmentation scheme was selected aiming only to reduce the purchase costs and to simplify the assembly procedure. The most convenient choice turned out consisting of using 8 identical arc-shaped PMs arranged in a 2 axial x 4 tangential array layout per each pole. Therefore, a total of $8 \times 7 = 56$ individual PMs were required to fully equip the hybrid exciter, each one featuring an axial length equal to 25mm , an angular span of 3.71° and a radial thickness of 1mm . A picture

comparing a PM to a coin is provided in Fig. 11a, highlighting the handy format achieved.

The PMs were then glued onto the machined gap-facing surfaces using an appropriate commercial epoxy resin. In Fig. 11b, an overview of the resulting stator arrangement is reported, whereas in Fig. 11c the detail of 3 teeth can be seen highlighting the consequent-pole layout adopted.

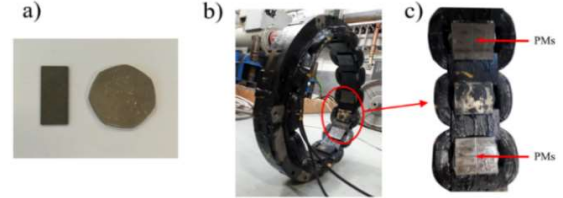


Fig. 11. Prototype exciter: a) arc-shaped bonded NdFeB PM, b) exciter stator after milling and gluing of the PMs, c) zoom-in on 3 stator teeth.

B. Experimental platform

After completion of the hybrid exciter stator prototype, it was assembled back into the available industrial genset that it had been taken from. The modified genset was then installed onto a test rig to permit investigating its operation, obtaining the experimental setup sketched in Fig. 12. The MA was mechanically coupled via a 10kNm torque-speed transducer to an 800kW induction machine (IM), which was properly supplied by a dedicated drive fed by the power grid to make it operate as the prime mover in either speed- or torque-control modes. The MA armature was also electrically connected to the power grid via a suited contactor, permitting to carry out both no-load tests when left open and on-load tests when closed, thus implementing the power recirculation test concept. A set of brushes and slip rings was also purposely installed at the back of the genset to permit both to disconnect at will the MA field winding from the rotating rectifier output and to record the most significant quantities related to the rotating windings, i.e. the line-to-line output voltages of the exciter and the voltage and current of the MA field winding. A general overview of the experimental test bench is shown in Fig. 13.

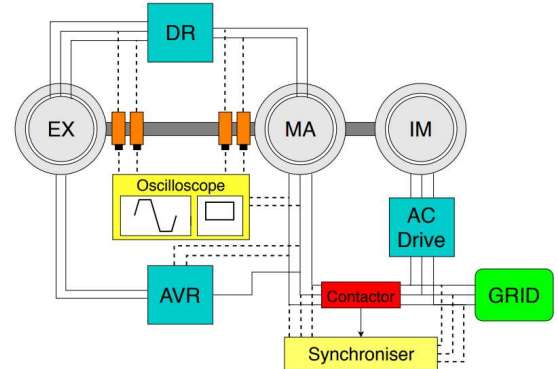


Fig. 12. Schematic of the experimental setup.

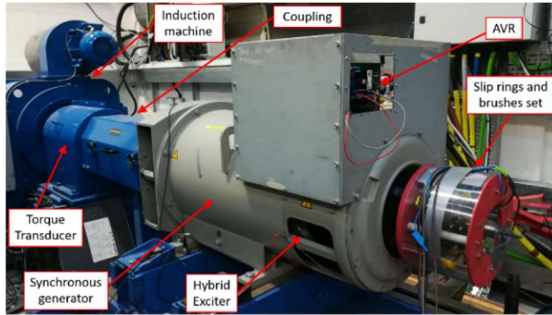


Fig. 13. Overview of the experimental setup.

C. Experimental tests

The hybrid exciter prototype was characterized by performing 3 types of tests, as detailed below.

- 1) No-load operation of the exciter. In this test, the genset speed is kept at the rated value $1500rpm$ by the induction drive operating in speed-control mode. The exciter field winding current is provided by a DC power supply operating in current control mode, whereas its armature currents are null since the field winding of the MA is disconnected from the rotating rectifier output. The AVR and the MA armature winding are also left unused. In these conditions, the line-to-line armature voltage generated by the exciter and the related DC output voltage provided by the rectifier are measured.
- 2) No-load operation of the MA. In this test, the genset speed is still kept at its rated value by the induction drive operating in speed-control mode. The MA armature winding is left open, whereas its field winding is connected to the output of the rotating rectifier. The field current in the MA, and thus its no-load armature voltage, are then controlled indirectly by adjusting the field current in the exciter, which is still provided by the DC power supply operating in current-control mode. The exciter AC voltage and the MA field voltage and current are measured, as well as the MA armature voltage. The AVR is left unused.
- 3) On-load operation of the MA. The induction drive initially accelerates the genset up to the rated speed while the AVR provides the field current to the exciter monitoring the armature voltages of the MA. When all the conditions for grid connection are satisfied, the synchronizer closes the contactor to permit the MA working as generator feeding power to the mains. The induction drive is simultaneously switched to torque-control mode and its torque is then properly settled to operate the MA under different active load conditions. The AVR is switched to its secondary operation mode, acting as an adjustable power factor (p.f.) controller by regulating the exciter field current. Besides all the measurements listed for test type 2), output power, voltage, current and p.f. of the MA are also recorded, as well as the steady state temperature achieved in the exciter stator poles when the MA operates at rated load condition. The experimental data obtained from the above tests are presented and commented in the next sub-sections.

D. Model validation

A first significant check concerns the line-to-line voltage generated by the exciter at rated speed and null armature currents (i.e. no-load operation supported only by the PMs – test type 1). The corresponding voltage waveforms and low-

frequency amplitude spectra provided by the simulation model and by the experimental tests are compared in Fig. 14. Overall, a good match is observed, despite some minor discrepancies. These might be due to a number of reasons, including slight differences in the B-H curves of cores' and PMs' materials. In fact, the slight overestimation that can be seen in Fig. 14 for the FE results compared to the experimental data is confirmed by the comparison shown with continuous lines in Fig. 15, where the field current is increased from $0A$ to $3.2A$ to obtain the classical no-load voltage curve of the exciter, ranging from $\approx 40\%$ to $\approx 150\%$ of the rated voltage. This leads to conclude that, possibly, the PMs properties declared by the manufacturer and used in the FE model are slightly overrated. Nevertheless, the relative error never exceeds 4.5% at any field current value.

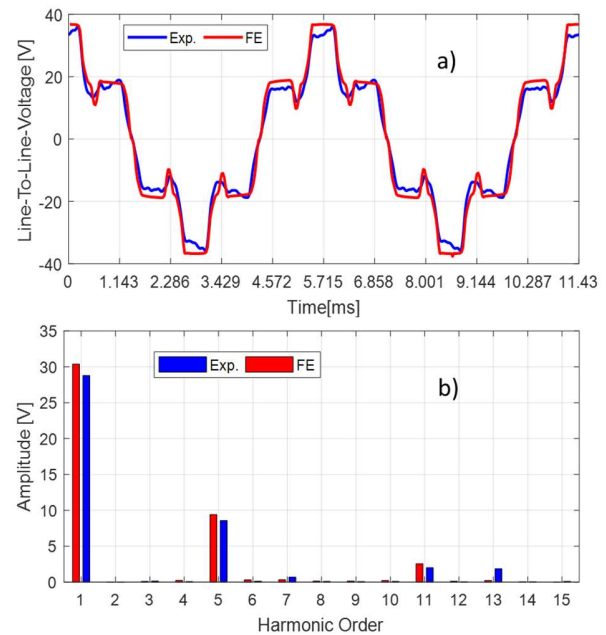


Fig. 14. Comparison between FE and experimental line-to-line voltage waveforms provided by the hybrid exciter at rated speed $1500rpm$ when its armature current is null: a) waveforms, b) spectra.

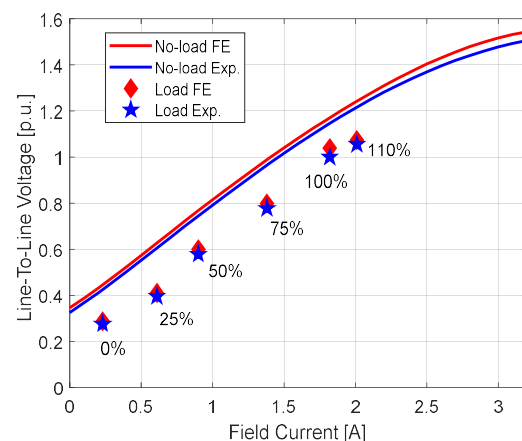


Fig. 15. Comparison between FE and experimental line-to-line RMS voltages provided by the exciter vs. its field current at rated speed: no-load curves (continuous lines); on-load results at various loading levels for the MA with p.f. 0.8 inductive (diamonds and stars).

For the sake of compactness, in Fig. 15 also the on-load results of the hybrid exciter are reported. The comparison between FE and experimental results is provided in terms of

p.u. line-to-line voltage for several significant operating conditions of the MA, i.e. 0%, 25%, 50%, 75%, 100% and 110% of the rated load with inductive p.f. equal to 0.8. Considering the overall agreement between such results, the accuracy of the simulation model is therefore further validated.

Among these MA loading levels, the 0% case, corresponding to the no-load operation of the MA at rated speed, is the most significant for the sake of this study, as it represents the reference scenario selected for sizing the PMs. Hence, for such operating condition, simulation results and experimental data concerning the average field current and the RMS armature voltage of the MA are compared for 2 levels of exciter field current, i.e. zero and a value that makes the MA generate approximately its rated voltage. The simulation results related to the MA field current were obtained via the model described in Section IV.E, whereas the corresponding output voltage values were obtained by using such current values in the 2D FE model of the same machine built for a previous investigation [2]. Overall, a very good agreement is obtained between numerical and experimental results, as shown in Table IV. As expected, when the exciter field current is null, the MA output voltage at no load is somewhat lower than its rated value ($\approx 15\%$), due to the final design choices adopted as described in Section IV.D.

TABLE IV
Comparison between FE and Experimental Results
for the MA No-Load Operation

	Exciter $I_{\text{field}} = 0.4A_{dc}$		Exciter $I_{\text{field}} = 0.23A_{dc}$	
	$I_{F,MA} [A_{dc}]$	$V_{ac,MA} [V_{rms}]$	$I_{F,MA} [A_{dc}]$	$V_{ac,MA} [V_{rms}]$
Simulation	10.1	342	14.1	406
Test	9.5	340	13.8	400
Error	5.9%	0.6%	2.1%	1.5%

VI. CONSIDERATIONS

The key advantage of the hybrid exciter concept vs. the benchmark machine consists in the lower m.m.f. required to its field winding. A full performance comparison between benchmark and hybrid exciters based on experimental data is reported in Table V for several significant operating conditions. For both platforms, the tests are run starting from room temperature and are carried out at practically cold conditions. As expected, the field current is significantly reduced in the hybrid exciter, with a decreasing benefit as the machine load level increases. However, an appreciable improvement is obtained even at 110% of rated load. When the resistance of the field winding is assumed to be the same for both machines, the related Joule losses are then reduced accordingly, as highlighted in Table V. This is also confirmed by the temperature of the exciter stator measured at steady state under full load conditions of the genset, which resulted $\approx 50^\circ\text{C}$ vs. $\approx 60^\circ\text{C}$ as measured in the benchmark machine. The over-temperature with respect to the external environment was then reduced by $\approx 10^\circ\text{C}$, i.e. about 25%, which is in good agreement with the estimated reduction of the Joule losses in the field winding.

TABLE V
Performance comparison for MA On-Load Operation

Loading % @ p.f. 0.8	Exciter Field Current $I_{f,exc} [A]$			Exciter Field Loss Reduction
	Benchmark	Hybrid	Reduction	

0%	0.64	0.23	64.1%	87.1%
25%	0.81	0.61	24.7%	43.3%
50%	1.21	0.90	23.8%	44.7%
75%	1.68	1.38	17.9%	32.5%
100%	2.21	1.82	17.7%	32.2%
110%	2.38	2.01	15.6%	28.7%

The reliability of the considered genset would be significantly improved when the proposed hybrid exciter was used. In fact, in case of full failure zeroing the exciter field current, the benchmark genset would go out of service whereas in the hybrid version the MA would still be able to supply the load, thanks to the excitation provided by the PMs, yet losing the voltage regulation capability. In addition, the lower temperature achieved in the exciter can affect favorably the reliability of the whole genset, possibly turning into a longer lifetime. Also, the reduction of the maximum current required for the field winding may permit to reduce the AVR stress.

The loss reduction in the field winding due to the presence of PMs also increases the efficiency of the exciter from $\approx 78.2\%$ **Error! Reference source not found.** to $\approx 78.6\%$ when operating at rated load, ultimately improving also the efficiency of the whole genset. Despite the efficiency figure exhibits a numerical improvement that can appear modest, the reduction of the exciter losses can result in not-negligible operational and economic advantages in a long-term perspective. In fact, even a limited reduction of losses could provide appreciable cumulated benefits along the entire lifetime of the genset, especially when long periods of continuous operation are expected, such as for the considered industrial case study.

Another important benefit of the proposed hybrid exciter is the improved voltage build-up at start-up. In fact, since the AVR is fed by the MA output, the benchmark genset relies only upon the residual magnetism in the cores to self-excite. This means that the voltage build-up is not always successful in such genset, as also confirmed by the industrial partner. On the other hand, in the hybrid exciter the PMs provide a basic excitation level even at null field current, thus ensuring a fast, reliable and always successful voltage build-up as soon as the genset is accelerated by the prime mover.

Additionally, the larger equivalent magnetic gap compared to the benchmark machine is expected to determine a smaller value of the field winding self-inductance as well as of the mutual inductance vs. armature phases and of the equivalent d- and q-axis inductances of the armature winding. In turn, this results in an inherently smaller dependence of the rectified voltage on the current fed to the MA field winding, as well as in a faster dynamic response of the ES. Both aspects may be considered beneficial side effects and will be analyzed in more detail in a future paper.

The main potential drawback deriving from adopting a hybrid excitation solution for the exciter consists in the higher manufacturing cost due to the inclusion of PMs. However, the proposed solution based on a simple consequent-pole surface-mount arrangement minimizes the modifications of the existing design, and the real impact of any related extra cost could be mitigated or even overcompensated by the energy savings produced during the lifecycle of the genset.

VII. CONCLUSIONS

In this paper, the application of hybrid PM – field winding solutions for the excitation of the main exciters of classical self-powered brushless ESs for WFSGs has been proposed and analyzed. The key concept of such solution consists in introducing PMs as an additional field source able to provide a suited basic flux level in the exciter even when its field current is null. This results into a boost that adds-up to the field winding m.m.f. during any other operating condition of the MA, still permitting the AVR to control the genset operation via the field current.

As a case study, the proposed concept was applied to an available industrial 400kVA genset. The minimization of the impact on the design of the existing exciter, on the AVR and on the overall upgrade cost was assumed as a design target to achieve a potentially more realistic application from an industrial point of view. After some design iterations, a consequent-pole layout with bonded NdFeB magnets was adopted. A prototype of the designed solution was then built by modifying the exciter of the available genset, gluing the PMs on the gap-facing sides of half of the stator poles that were purposely milled. The genset was then assembled onto a purposely equipped test rig to carry out different tests. The experimental data obtained were compared to corresponding simulation results, confirming the expected operation and thus the benefits of the proposed hybrid solution, such as a reduction of the excitation power by over 30% at full-load of the MA. Therefore, the hybrid excitation was proved to be applicable to brushless exciters of industrial gensets, with multiple appreciable benefits and a minimal impact on their manufacturing process. This concept, although already in use in many electrical machines, was never exploited before for exciters of synchronous machines in such a comprehensive way, i.e. a full-scale prototype was built and tested for validation.

REFERENCES

- [1] A. E. Bell and P. Anpalahan, "Optimisation of Salient-Pole Rotor for Synchronous Generators," *2018 XIII International Conference on Electrical Machines (ICEM)*, Alexandroupoli, 2018, pp. 339-344, doi: 10.1109/ICELMACH.2018.8506805.
- [2] S. Nuzzo et al., "A Methodology to Remove Stator Skew in Small-Medium Size Synchronous Generators via Innovative Damper Cage Designs," *in IEEE Transactions on Industrial Electronics*, vol. 66, no. 6, pp. 4296-4307, June 2019, doi: 10.1109/TIE.2018.2864699.
- [3] A. Tassarolo, C. Bassi and D. Giulivo, "Time-Stepping Finite-Element Analysis of a 14-MVA Salient-Pole Shipboard Alternator for Different Damper Winding Design Solutions," *in IEEE Transactions on Industrial Electronics*, vol. 59, no. 6, pp. 2524-2535, June 2012, doi: 10.1109/TIE.2011.2157294.
- [4] S. Nuzzo, P. Bolognesi, C. Gerada and M. Galea, "Simplified Damper Cage Circuit Model and Fast Analytical-Numerical Approach for the Analysis of Synchronous Generators," *in IEEE Transactions on Industrial Electronics*, vol. 66, no. 11, pp. 8361-8371, Nov. 2019, doi: 10.1109/TIE.2018.2885737.
- [5] Geoff Klempner; Isidor Kerszenbaum, "Operation and Control," in *Handbook of Large Turbo-Generator Operation and Maintenance*, IEEE, 2018, pp.201-330, doi: 10.1002/9781119390718.ch4.
- [6] S. Nuzzo, M. Galea, C. Gerada and N. L. Brown, "Prediction of the voltage drop due to the diode commutation process in the excitation system of salient-pole synchronous generators," *2016 19th International Conference on Electrical Machines and Systems (ICEMS)*, Chiba, 2016, pp. 1-6.
- [7] S. Nuzzo, M. Galea, C. Gerada and N. Brown, "Analysis, Modeling, and Design Considerations for the Excitation Systems of Synchronous Generators," *in IEEE Transactions on Industrial Electronics*, vol. 65, no. 4, pp. 2996-3007, April 2018, doi: 10.1109/TIE.2017.2756592.
- [8] G. Laliberte, *A comparison of generator excitation systems (Power topic 6008-Technical information from Cummins Power Generation)*, Oct. 2014. [Online]. Available: <https://trienergy.com/wp-content/uploads/2017/10/Sistemas-de-Excitacion-en-Generadores.pdf>
- [9] C. M. Hansen Jr., A. W. Wohlberg, "Combination Exciter/Permanent Magnet Generator for Brushless Generator System", U.S. Patent 4,223,263, 1980.
- [10] J. K. Noland, S. Nuzzo, A. Tassarolo and E. F. Alves, "Excitation System Technologies for Wound-Field Synchronous Machines: Survey of Solutions and Evolving Trends," *in IEEE Access*, vol. 7, pp. 109699-109718, 2019, doi: 10.1109/ACCESS.2019.2933493.
- [11] E. Spooner, S. A. W. Khatib and N. G. Nicolaou, "Hybrid excitation of AC and DC machines," *1989 Fourth International Conference on Electrical Machines and Drives Conf. Publ. No. ??*, London, UK, 1989, pp. 48-52.
- [12] J. F. Gieras, "PM synchronous generators with hybrid excitation systems and voltage control Capabilities: A review," *2012 XXth International Conference on Electrical Machines*, Marseille, 2012, pp. 2573-2579, doi: 10.1109/ICEIMach.2012.6350248.
- [13] J-C. Matt, J-C. Mipo, A. Foggia, "Synchronous Rotary Electric Machine having a Hybrid-Excitation Rotor", U.S. 9,197, 118 B2, 2015.
- [14] H. Hua, Z. Q. Zhu and H. Zhan, "Novel Consequent-Pole Hybrid Excited Machine With Separated Excitation Stator," *in IEEE Transactions on Industrial Electronics*, vol. 63, no. 8, pp. 4718-4728, Aug. 2016, doi: 10.1109/TIE.2016.2559447.
- [15] A. Dupas, S. Hlioui, E. Hoang, M. Gabsi and M. Lecrivain, "Investigation of a New Topology of Hybrid-Excited Flux-Switching Machine With Static Global Winding: Experiments and Modeling," *in IEEE Transactions on Industry Applications*, vol. 52, no. 2, pp. 1413-1421, March-April 2016, doi: 10.1109/TIA.2015.2497305..
- [16] M. Onsal, Y. Demir and M. Aydin, "A New Nine-Phase Permanent Magnet Synchronous Motor With Consequent Pole Rotor for High-Power Traction Applications," *in IEEE Transactions on Magnetics*, vol. 53, no. 11, pp. 1-6, Nov. 2017, Art no. 8700606, doi: 10.1109/TMAG.2017.2709788.
- [17] J. Pyrhonen, J. Tapani, and V. Hrabovcova, `Design of Rotating Electrical Machines. Chichester, U.K.: Wiley, 2008.
- [18] P. Bolognesi, "A mid-complexity analysis of long-drum-type electric machines suitable for circuit modeling," *2008 18th International Conference on Electrical Machines*, Vilamoura, 2008, pp. 1-5, doi: 10.1109/ICELMACH.2008.4799879..
- [19] G. Decuzzi, S. Nuzzo, P. Bolognesi, P. Giangrande and M. Galea, "Hybrid Magnet - Field Winding Solutions for Exciters of Synchronous Generators," *2019 IEEE International Electric Machines & Drives Conference (IEMDC)*, San Diego, CA, USA, 2019, pp. 1458-1463, doi: 10.1109/IEMDC.2019.8785174.